REPORT DOCUMENTATION PAGE

Form Approved OMB NO. 0704-0188

1. REPORT DATE (DD-MM-YYYY)	2. REPORT TYPE	3. DATES COVERED (From - To)
	New Reprint	-

4. TITLE AND SUBTITLE
Exfoliation and Reassembly of Cobalt Oxide Nanosheets into a Reversible Lithium-Ion Battery Cathode

5a. CONTRACT NUMBER
W911NF-09-1-0541

5b. GRANT NUMBER

5c. PROGRAM ELEMENT NUMBER
611103

6. AUTHORS
Owen C. Compton, Ali Abouimrane, Zhi An, Marc J. Palmeri, L. Catherine Brinson, Khalil Amine, SonBinh T. Nguyen

5d. PROJECT NUMBER

5e. TASK NUMBER

5f. WORK UNIT NUMBER

7. PERFORMING ORGANIZATION NAMES AND ADDRESSES
Northwestern University Evanston Campus
Office for Sponsored Research (OSR)
1801 Maple Ave.
Evanston, IL 60201 -

8. PERFORMING ORGANIZATION REPORT NUMBER

9. SPONSORING/MONITORING AGENCY NAME(S) AND ADDRESS(ES)
U.S. Army Research Office
P.O. Box 12211
Research Triangle Park, NC 27709-2211

10. SPONSOR/MONITOR'S ACRONYM(S)
ARO

11. SPONSOR/MONITOR'S REPORT NUMBER(S)
56159-CH-MUR.24

12. DISTRIBUTION AVAILIBILITY STATEMENT
Approved for public release; distribution is unlimited.

13. SUPPLEMENTARY NOTES
The views, opinions and/or findings contained in this report are those of the author(s) and should not contrued as an official Department of the Army position, policy or decision, unless so designated by other documentation.

14. ABSTRACT
An exfoliation–reassembly–activation (ERA) approach to lithium-ion battery cathode fabrication is introduced, demonstrating that inactive HCoO2 powder can be converted into a reversible Li1-xHxCoO2 thin-film cathode. This strategy circumvents the inherent difficulties often associated with the powder processing of the layered solids typically employed as cathode materials. The delamination of HCoO2 via a combination of chemical and mechanical exfoliation generates a highly processable aqueous dispersion of [CoO2]? nanosheets that is critical to

15. SUBJECT TERMS
exfoliation, reassembly, battery fabrication, cobalt oxide

16. SECURITY CLASSIFICATION OF:			17. LIMITATION OF ABSTRACT	15. NUMBER OF PAGES	19a. NAME OF RESPONSIBLE PERSON
a. REPORT	b. ABSTRACT	c. THIS PAGE			Horacio Espinosa
UU	UU	UU	UU		19b. TELEPHONE NUMBER: 847-/46-7598

Standard Form 298 (Rev 8/98)
Prescribed by ANSI Std. Z39.18

Report Title

Exfoliation and Reassembly of Cobalt Oxide Nanosheets into a Reversible Lithium-Ion Battery Cathode

ABSTRACT

An exfoliation–reassembly–activation (ERA) approach to lithium-ion battery cathode fabrication is introduced, demonstrating that inactive HCoO2 powder can be converted into a reversible Li1-xHxCoO2 thin-film cathode. This strategy circumvents the inherent difficulties often associated with the powder processing of the layered solids typically employed as cathode materials. The delamination of HCoO2 via a combination of chemical and mechanical exfoliation generates a highly processable aqueous dispersion of [CoO2]? nanosheets that is critical to the ERA approach. Following vacuum-assisted self-assembly to yield a thin-film cathode and ion exchange to activate this material, the generated cathodes exhibit excellent cyclability and discharge capacities approaching that of low-temperature-prepared LiCoO2
(~83 mAh g?1), with this good electrochemical performance attributable to the high degree of order in the reassembled cathode.

REPORT DOCUMENTATION PAGE (SF298)
(Continuation Sheet)

Continuation for Block 13

ARO Report Number 56159.24-CH-MUR
Exfoliation and Reassembly of Cobalt Oxide Nan ...

Block 13: Supplementary Note

Approved for public release; distribution is unlimited.

Exfoliation and Reassembly of Cobalt Oxide Nanosheets into a Reversible Lithium-Ion Battery Cathode

*Owen C. Compton, Ali Abouimrane, Zhi An, Marc J. Palmeri, L. Catherine Brinson, Khalil Amine, and SonBinh T. Nguyen**

An exfoliation–reassembly–activation (ERA) approach to lithium-ion battery cathode fabrication is introduced, demonstrating that inactive $HCoO_2$ powder can be converted into a reversible $Li_{1-x}H_xCoO_2$ thin-film cathode. This strategy circumvents the inherent difficulties often associated with the powder processing of the layered solids typically employed as cathode materials. The delamination of $HCoO_2$ via a combination of chemical and mechanical exfoliation generates a highly processable aqueous dispersion of $[CoO_2]^-$ nanosheets that is critical to the ERA approach. Following vacuum-assisted self-assembly to yield a thin-film cathode and ion exchange to activate this material, the generated cathodes exhibit excellent cyclability and discharge capacities approaching that of low-temperature-prepared $LiCoO_2$ (~83 mAh g^{-1}), with this good electrochemical performance attributable to the high degree of order in the reassembled cathode.

1. Introduction

Lithium-ion batteries (LIBs) are the power source of choice for portable consumer electronic devices given their superior energy density per unit weight (Wh kg^{-1}) and unit volume (Wh l^{-1}) in comparison to alternative battery technologies (e.g., Pb-acid, Ni-Cd, NiMH).[1,2] The operation of LIBs relies primarily upon the reversible migration of Li ions between electrodes, which are insertion compounds.[3] These compounds typically possess layered structures to facilitate the frequent Li ion intercalation and deintercalation processes during charging and discharging, with graphite and layered metal oxides being the most commonly studied anode and cathode materials, respectively.[4] Although a wide variety of compositions have been employed as potential cathode materials, $LiCoO_2$ has been developed as one of the primary cathodes for commercial batteries given its high energy density, easy preparation, and excellent structural stability.[5]

In spite of their good electrochemical properties, $LiCoO_2$ and other metal oxide cathode materials are powdered solids, which are inherently difficult to handle and process.[6] Highly flexible solution-processing techniques cannot be directly applied to such powders due to their insolubility in all solvents, while their poor thermal stability in a partially delithiated state (≈250 °C decomposition temperature for Li_xCoO_2)[7] excludes melt processing.[8] Fortunately, the advent of exfoliation as a strategy for preparing colloidal dispersions of layered powdered solids, via either chemical or mechanical means, offers an indirect solution to circumvent such processing difficulties. Indeed, aqueous and organic dispersions comprising single nanosheets or few-layer aggregates have been prepared from layered solids like graphite,[9] clay,[10] perovskites,[11] and most recently, metal chalcogenides/oxides.[12] Such dispersions are similar to true solutions and

Dr. O. C. Compton, Z. An, Prof. S. T. Nguyen
Department of Chemistry
Northwestern University
2145 Sheridan Road, Evanston, IL 60208-3113, USA
E-mail: stn@northwestern.edu
Dr. O. C. Compton, Dr. A. Abouimrane, Dr. K. Amine, Prof. S. T. Nguyen
Chemical Sciences and Engineering Division
Argonne National Laboratory
9700 South Cass Avenue, Argonne, IL 60439, USA
M. J. Palmeri, Prof. L. C. Brinson
Departments of Materials Science and Engineering and Mechanical Engineering
Northwestern University
2145 Sheridan Road, Evanston, IL 60208-3113, USA

DOI: 10.1002/smll.201101131

NANO MICRO small

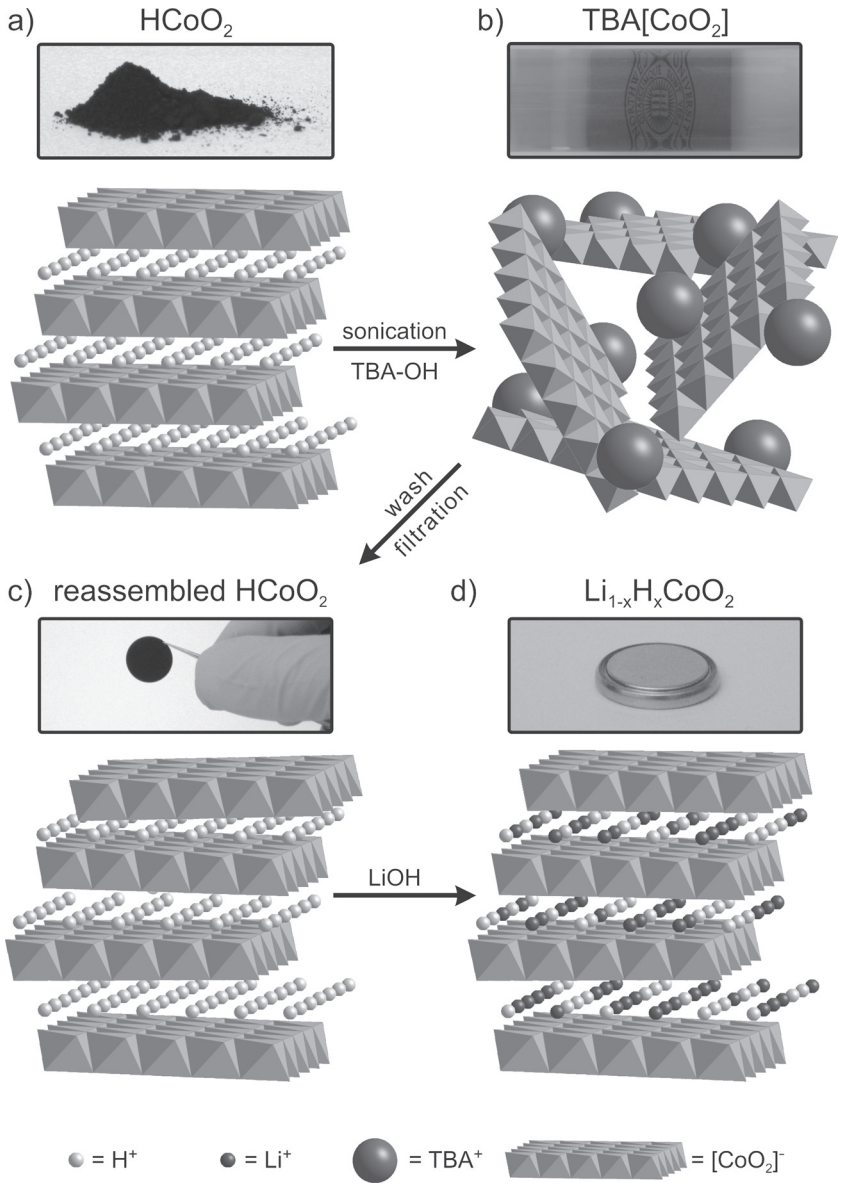

Figure 1. A schematic illustration of the exfoliation and reassembly of $[CoO_2]^-$ nanosheets into an electrochemically active cathode. In each panel, the corresponding structure of the layered material is shown underneath the digital image. All structural components are labeled in the legend at the bottom of the figure. a) Top: A digital image of $HCoO_2$ powder. b) Top: A digital image of the cross-section of a vial containing an aqueous dispersion of $[CoO_2]^-$ nanosheets. As apparent by the seal of Northwestern University in the background, this dispersion is optically clear and efficiently scatters light, as demonstrated by the Tyndall effect on a laser (left side of image). a,b) Bottom: The exfoliated nanosheets are illustrated along with the TBA exfoliant. c) Top: A digital image of a VASA-fabricated self-supporting thin film of $HCoO_2$. d) Top: A digital image of the CR-2032 coin-type cell used in the testing of the $Li_{1-x}H_xCoO_2$ cathode. c,d) Bottom: Introduction of Li^+ into $HCoO_2$ film via ion exchange yields an electrochemically active material that can function reversibly as a cathode in this cell. Incomplete replacement of inactive H^+, as shown in the corresponding structure, limits the overall capacity. A color reproduction of this figure is available in the SI (Figure S6).

have been used successfully in the fabrication of nanosheet-based thin films using standard solution-processing methods such as layer-by-layer assembly,[13] spin-coating,[14] and vacuum-assisted self-assembly (VASA),[15,16] among others.

Herein, we present the exfoliation of cobalt oxide nanosheets ($[CoO_2]^-$) into nanosheet dispersions that can be reassembled and chemically modified into electrochemically active $Li_{1-x}H_xCoO_2$ thin-film cathodes with excellent discharge capacities and good cyclabilities. This exfoliation-reassembly-activation (ERA) approach to cathode fabrication introduces a high degree of processability that was previously inaccessible to CoO_2-based powdered solids. Such flexibility in processing opens the door to the preparation of hybrid cathodes, where the reassembled metal oxide nanosheets can serve as a matrix for the incorporation of additives[12] to enhance the conductivity, capacity, or cyclability of the reassembled cathode above that of the parent powdered solid. Since many other layered metal oxides with different compositions have been identified as active cathodic materials, the ERA fabrication technique should allow for the facile production of myriad thin film cathodes.

2. Results and Discussion

2.1. Method of Exfoliation

The key step in generating a solution-processable dispersion of $[CoO_2]^-$ nanosheets lies in the successful exfoliation of powdered $HCoO_2$ solid. This delamination process was achieved via a combination of chemical and mechanical exfoliation (**Figure 1**) in the presence of tetrabutylammonium (TBA) hydroxide, where intercalation of the sterically large TBA cation into the interlayer gallery was promoted with ultrasonication as well as neutralization of the acidic proton sites. Upon penetration into the $HCoO_2$ structure, the sterically large TBA cation (hydrodynamic radius ≈ 4.8 Å)[17] migrates through the tightly packed intersheet gallery (≈2.6 Å),[18] displaces hydrogen atoms and separates adjacent layers to produce the desired $[CoO_2]^-$ nanosheet product. We note that the necessity of a sonication step in our preparation indicates that the radius of TBA is too large to efficiently penetrate the $HCoO_2$ structure without an adequate driving force. Upon displacement, the extracted H^+ is neutralized by excess hydroxide in the solution that serves as a counter ion to the TBA. We suspect that the formation of water is a key step to successful exfoliation, as attempts to produce $[CoO_2]^-$ nanosheets using different combinations of reactants, such as $LiCoO_2$/TBA-OH, $LiCoO_2$/LiOH, and $HCoO_2$/TBA-Br, were unsuccessful.

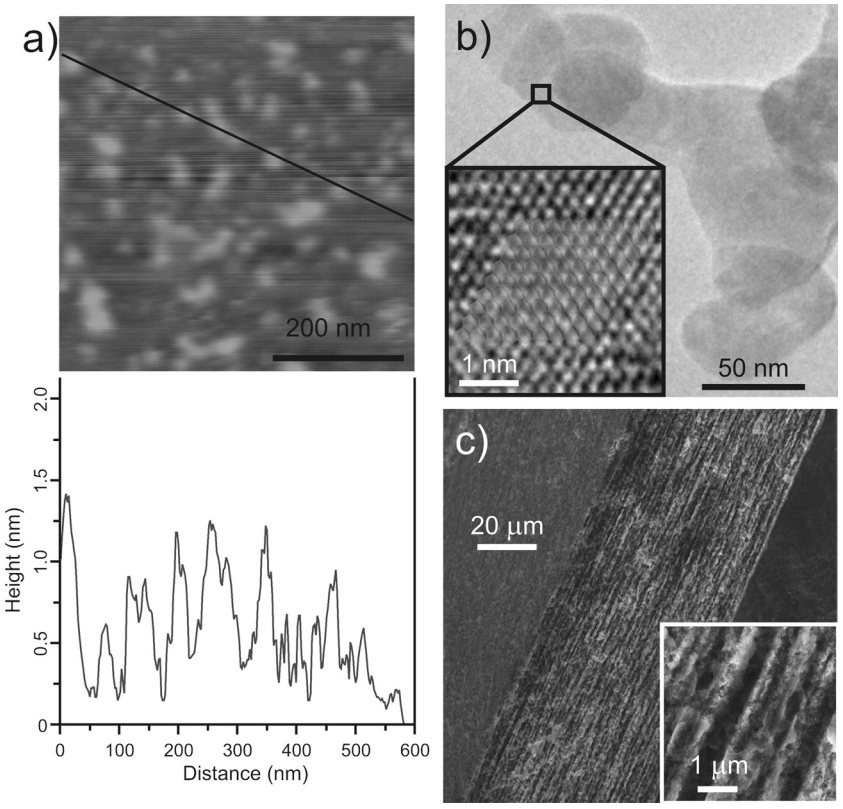

Figure 2. a) Top: An AFM image of $[CoO_2]^-$ nanosheets that were drop-cast from a $HCoO_2$ dispersion onto a mica substrate. Bottom: The corresponding height scan reveals the presence of individual sheets (≈0.35 nm in thickness), along with bi- and trilayer aggregates. b) A bright-field HRTEM image of $[CoO_2]^-$ nanosheets that were drop-cast from a $HCoO_2$ dispersion onto a TEM grid, showing overlapping nanosheets. The inset is a magnified HRTEM image that illustrates the hexagonal close-packed arrangement of cobalt atoms (black dots) in the sheet structure with a model of the edge-sharing CoO_6 octahedra overlaid for clarity. c) A scanning electron microscopy (SEM) image of the lamellar structure of a reassembled $HCoO_2$ thin film. The inset illustrates the relative homogeneity of the structure at the microscale. A color reproduction of this figure is available in the SI (Figure S7).

After exfoliation, the as-synthesized $[CoO_2]^-$ nanosheets are copiously washed with water to remove residual TBA. The resulting aqueous $[CoO_2]^-$ dispersions (TBA content = 1.67 wt% as determined by combustion analysis; other TBA-stabilized metal oxide formulations can have up to 12 wt% TBA[19]) are stable for up to 6 months as H^+-stabilized nanosheets.[20] Presumably, TBA only serves to separate the nanosheets from each other during exfoliation. After washing, residual protons from the aqueous dispersion were enough to neutralize the surface charge of the nanosheets without the need for TBA counterions and the dispersed sheets again possess the electrochemically inactive composition of $HCoO_2$.

2.2. Characterization of Exfoliated Sheet

While the preparation of a stable dispersion is an excellent indicator of exfoliation, the delamination of $[CoO_2]^-$ into individual nanosheets, not just multilayer aggregates, was confirmed using both atomic force microscopy (AFM) and high-resolution transmission electron microscopy (HRTEM). In an AFM image (**Figure 2**a), single $[CoO_2]^-$ sheets appear as ≈4 Å-thick platelets, whereas the expected thickness from the crystal structure is 2.1 Å.[18] A similar discrepancy in nanosheet thickness has been observed with single-layer graphene, whose 3.4 Å thickness is artificially increased to ≈8–10 Å when imaged with AFM.[21] An HRTEM image of a single $[CoO_2]^-$ nanosheet (Figure 2b) reveals the hexagonal close-packing of edge-shared cobalt oxide octahedra, where the cobalt atoms are depicted as dark circles. A simulated crystal structure for a single $[CoO_2]^-$ sheet overlays precisely with the observed structure from the HRTEM image, further confirming that individual sheets can be successfully exfoliated via our methodology. The lateral dimensions of these nanosheets are approximately 100 nm as measured by dynamic light scattering (DLS, see Figure S1 in the Supporting Information (SI) for size distribution curve). This value is slightly larger than expected from the AFM and HRTEM images, as DLS monitors the hydrodynamic diameter of the nanosheets and not their physical dimension.

Although single nanosheets were clearly observed by both microscopy techniques, some multi-layer aggregates were also found in these images. Profile scans of AFM images reveal the presence of bi- and trilayer aggregates featuring discrete platelet heights of ≈7 and ≈11 Å, respectively. Such multilayer structures are also distinguishable via HRTEM (Figure S2 in SI) as regions containing what appear to be lines of Co atoms, which result from the staggered ABC arrangement of the unexfoliated nanosheets.[22] These multilayer structures presumably account for the larger particles that are sometimes found to settle out of the dispersion upon prolonged standing.[20]

2.3. Fabrication and Activation of Reversible Cathode

To prepare binder-free LIB cathodes from the aforementioned aqueous dispersion of $[CoO_2]^-$ nanosheets, we employed the quick, inexpensive, and facile VASA method, which has been successfully utilized to prepare thin films from a wide variety of 2D nanoparticles including reduced graphene oxide[15] and silicate clay.[23] Reassembly of $[CoO_2]^-$ on a membrane yields a self-supporting thin film that can be isolated for further manipulation. While this $HCoO_2$ film is still electrochemically inactive at this stage in our fabrication protocol, it is important to note that the direct fabrication of such a film from the parent powdered solid is inaccessible under traditional processing methods. Scanning electron microscope (SEM) images of this VASA-assembled film reveal an ordered, lamellar structure (Figure 2c) with a few

NANO MICRO small

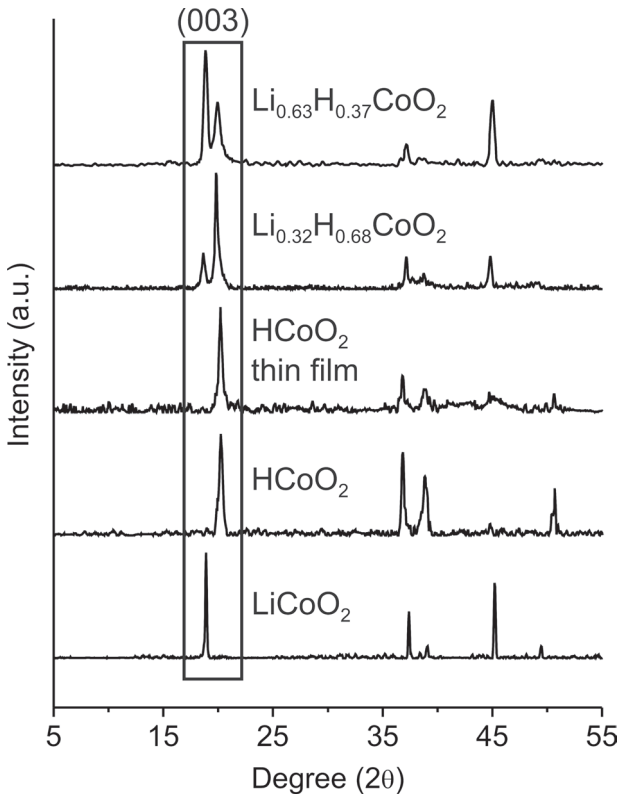

Figure 3. PXRD patterns illustrating the structural changes that occur during the processing of our ERA materials, from the parent $HCoO_2$ powder to the ion-exchanged $Li_{1-x}H_xCoO_2$ thin film. Most distinctly, patterns for $HCoO_2$ before exfoliation (second pattern from the bottom) and after reassembly (third pattern from the bottom) exhibit a (003) reflection near $2\theta = 20.3°$, while this same reflection is near $2\theta = 18.9°$ for commercially purchased $LiCoO_2$ (bottom pattern). Both of these reflections are present in patterns of the ion-exchanged cathodes (top two patterns), with the ratio of these peaks being dependent on the extent of Li^+ intercalation. All patterns have been normalized to the intensity of the strongest of the two (003) reflections. Complementary PXRD patterns with all reflections labeled are available in the SI (Figure S4).

heterogeneities and vacancies apparent at higher magnification (Figure 2c inset). Such minor inconsistencies in the thin film structure could be attributed to the presence of a small amount of the aforementioned multilayer aggregates that likely disrupt order during fabrication. Powder X-ray diffraction (PXRD) further confirms the successful reassembly of $HCoO_2$ nanosheets, with a characteristic (003) reflection at $2\theta = 20.3°$ that corresponds to the gallery spacing in crystalline $HCoO_2$ (**Figure 3**).[24]

To activate the reassembled $HCoO_2$ thin film for electrochemical cycling, we employed a cation exchange strategy that was first proposed by Larcher et al.,[25] where treating the material in aqueous LiOH solution would convert the proton sites in the film to water and fill the vacated positions within the gallery of the structure with Li^+ ions. At moderate temperature and pressure (90 °C and 1 bar), no quantifiable exchange occurs for our reassembled $HCoO_2$ film; however, significant amounts of Li^+ can be loaded into it at higher temperature and pressure (160 °C and 60 bar). At high LiOH concentration (2.5 M), an active cathode film with a composition of $Li_{0.63}H_{0.37}CoO_2$ was generated after 5 days. Reducing the LiOH concentration by tenfold elicited less ion exchange and yielded an active cathode with a composition of $Li_{0.32}H_{0.68}CoO_2$, thus demonstrating that ion exchange can be easily controlled by varying Li^+ concentration in the exchange medium.

Successful ion exchange in the aforementioned thin-film cathodes was further verified by powder X-ray diffraction (PXRD), where two distinct (003) reflections corresponding to $LiCoO_2$ and $HCoO_2$ ($2\theta = 18.9°$ and 20.3°, respectively)[18,24] were observed (Figure 3, see Figure S4 and Table S1 in SI for fully labeled patterns). Notably, the extent of ion exchange can be determined by the ratio of the intensities at 18.9° (I_{Li}) and 20.3° (I_H), with $Li_{0.63}H_{0.37}CoO_2$ having an I_{Li}/I_H ratio of 1.82; as a comparison, this ratio is only 0.32 for $Li_{0.32}H_{0.68}CoO_2$. That two resolvable peaks for the (003) reflection exist in the PXRD pattern, rather than a single coalesced peak, suggests the presence of segregated domains containing only H^+ or Li^+ in the ion-exchanged structure. Such a result may be attributed to multidomain aggregates in the cathode, where certain proton sites (i.e., those between unexfoliated nanosheets) are much more difficult to extricate from the structure in comparison to others (i.e., those found at the interface between two reassembled $[CoO_2]^-$ sheets).

2.4. Electrochemical Performance and Cathode Order

Both the $Li_{0.63}H_{0.37}CoO_2$ and $Li_{0.32}H_{0.68}CoO_2$ cathodes exhibited charge/discharge profiles against Li/Li^+ (**Figure 4**a) that are quite similar to that reported for pristine $LiCoO_2$,[26] with distinguishable voltage plateaus near 3.9 V during the discharge phase. The initial discharge capacity of the $Li_{0.63}H_{0.37}CoO_2$ cathode was 74 mAh g^{-1}, nearly 90% of that (≈83 mAh g^{-1}) observed for low temperature (LT)-$LiCoO_2$ (i.e., prepared at 400 °C).[27] The slightly lower capacity value for our thin film cathode could be attributed primarily to incomplete ion exchange, where inactive H^+ remains in the structure and limits the available amount of Li^+ in the cathode. Indeed, the $Li_{0.32}H_{0.68}CoO_2$ cathode with less intercalated Li^+ had a much lower initial discharge capacity (48 mAh g^{-1}) than the $Li_{0.63}H_{0.37}CoO_2$ cathode. Thus, further development of the ion exchange step to completely remove the inactive proton sites from the cathode structure would be critical to maximizing electrochemical performance.

The good order within the structures of our $Li_{0.63}H_{0.37}CoO_2$ and $Li_{0.32}H_{0.68}CoO_2$ cathodes, as qualitatively suggested by their sharp, intense PXRD patterns (Figure 3), may be a contributing factor to their excellent capacity values. Indeed, the low performance of $LiCoO_2$ cathodes containing a significant amount of defects has been attributed to the slow migration kinetics of Li^+ into and out of the disordered cathode layers.[28] Since the facile kinetics of Li^+ transportation into and out of the $LiCoO_2$ structure during cycling has been identified as key to improved electrochemical properties of this material,[29] the organized structure of the $[CoO_2]^-$ nanosheets in our ERA cathodes is vital to the good reversible capacity of this material.

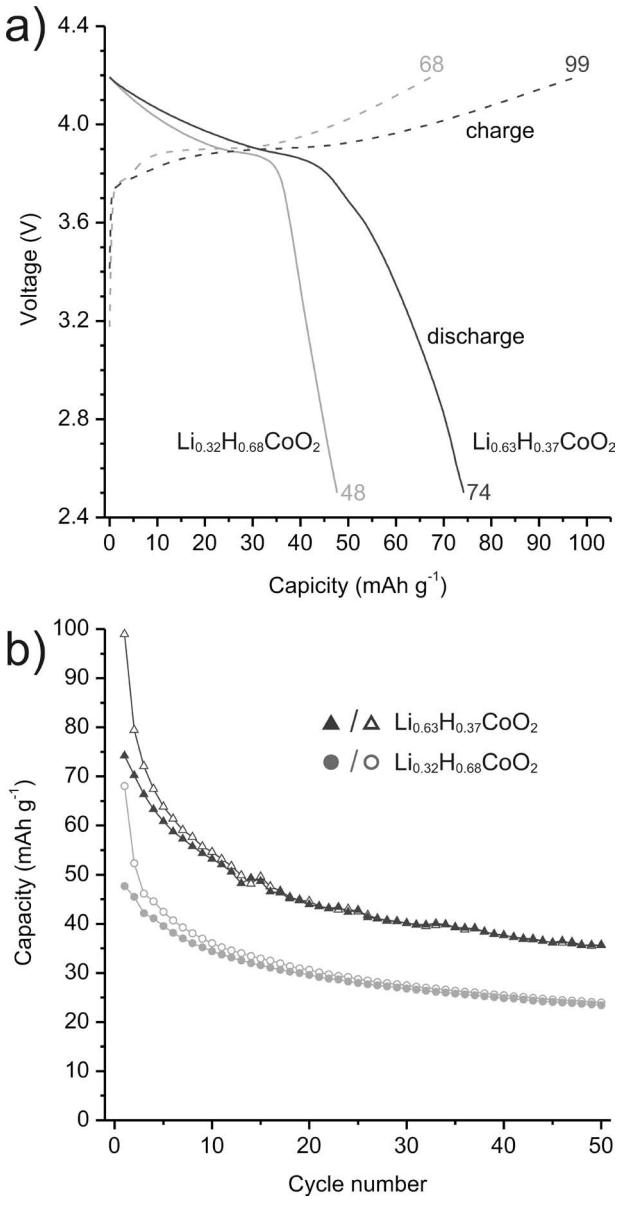

Figure 4. a) Initial charge–discharge profiles of $Li_{1-x}H_xCoO_2$ cathodes, demonstrating that capacity can be enhanced by incorporating more active Li^+ into the thin film structure. Charge profiles are represented as dashed lines, while discharge curves are solid. b) A plot of charge (empty symbols) and discharge (solid symbols) capacities during cycling illustrates the good retention of electrochemical properties for our $Li_{1-x}H_xCoO_2$ cathodes over time. All data were collected at a current rate of 20 mAh g^{-1}.

To quantify the degree of order in our ERA electrodes, we compared the X-ray scattering coherence lengths perpendicular to the lamellar order in their structures. These values can be estimated by applying the Scherrer formula[30] (Equation S1 in SI) to the (003) reflection in the PXRD patterns of the $Li_{1-x}H_xCoO_2$ species (Figure 3). Discounting the 2θ = 20.3° component of this reflection and utilizing only the signal at 2θ = 18.9°, this formula reveals that ordering of $[CoO_2]^-$ nanosheets extends for ≈40 Å for both $Li_{0.63}H_{0.37}CoO_2$ and $Li_{0.32}H_{0.68}CoO_2$ cathodes, which correlates to approximately ten contiguous layers with no disorder! Such a high degree of order is remarkable in comparison to pristine high-temperature (HT)-$LiCoO_2$ (i.e., prepared at or above 850 °C),[5,31] which features around twenty contiguous ordered layers, in spite of the much higher annealing temperatures employed to achieve this crystalline structure.

In addition to its excellent capacity values, the reassembled $Li_{0.63}H_{0.37}CoO_2$ material also exhibits good cyclability. While significant irreversible capacity was observed in the first cycle (Figure 4a), which should be attributed to the formation of a solid-electrolyte interphase (SEI) layer,[32] Coulombic efficiency (i.e., the% ratio of charge to discharge capacity) was remarkably high from the second cycle forward with an average value of 99% over the course of 50 cycles. Although cycling over this period increased the efficiency of the cathode, capacity gradually declined to a final discharge capacity of 36 mAh g^{-1}. Similar declines in performance after repeated cycling have been observed for pristine $LiCoO_2$[31] and other layered metal oxide cathodes like $LiMnO_2$[33] and $LiNiO_2$,[34] where structural disorders caused by continuous lithiation and delithiation have been identified as primary contributing factors to decreases in performance. These structural changes are also likely the case for the decreased performance of our ERA cathode upon recycling.

3. Conclusion

We have presented a facile technique for the exfoliation of $[CoO_2]^-$ to yield aqueous dispersions that can be reassembled via solution-processing techniques and activated into a reversible LIB cathode. Such cathodes exhibit excellent cyclability with initial discharge capacities reaching 74 mAh g^{-1}, nearly 90% of that observed for pristine LT-$LiCoO_2$ (83 mAh g^1).[27] As discharge capacity was found to vary with Li^+ content in the cathode, and our most successful exchange still left nearly one third of inactive proton sites in the cathode structure, optimization of the ion-exchange step should lead to performance that surpasses the properties of pristine HT-$LiCoO_2$ (120 mAh g^{-1}).[31] That such good electrochemical performance can be achieved with a solution-processable cathode film prepared at a relatively low temperature (≈160 °C) is a significant advancement in cathode fabrication, since high-performance LIB cathodes typically require a high-temperature (>800 °C) preparation of difficult-to-process powdered solids as the first step.

Because the structure of our ERA cathode is nearly identical to that of pristine $LiCoO_2$, traditional strategies for enhancing the electrochemical performance of $LiCoO_2$ cathode, such as the application of coatings[35,36] or dopants,[37] should lead to similar improvements in our reassembled cathode. As an added benefit, the processing flexibility afforded by nanosheet delamination and reassembly should enable solution-based incorporation of additives into the reassembled cathode: the additive particle can simply be dispersed along with the nanosheets and co-assembled during VASA to yield a hydbrid cathode.[12] Finally, given that the majority of LIB cathode materials are layered metal oxides, our exfoliation-reassembly-activation strategy should also be readily extendable to these materials.

NANO MICRO small

4. Experimental Section

Synthesis of Crystalline $HCoO_2$: $HCoO_2$ was prepared according to a modified literature procedure.[38] Briefly, $CoCl_2 \cdot 6H_2O$ (4 g) was dissolved in water (50 mL) to give a deep pink solution. While this solution was being stirred, aqueous NaOH (50 mL of a 4 M solution) was added, producing an initially blue precipitate of α-$Co(OH)_2$ that turned into the rose-pink β-$Co(OH)_2$ at the end of the addition.[39] The pink β-$Co(OH)_2$ precipitate was isolated from solution via centrifugation (15 min at 8200 g) and subjected to two cycles of [resuspension in ultrapure deionized water (40 mL) + centrifugation (15 min at 8200 g) + decantation] to remove the excess salts. The isolated pink precipitate was then resuspended in ultrapure deionized water (100 mL) and stirred vigorously overnight under a slowly bubbling stream of O_2 (the tip of the bubbling needle is under the surface of the suspension). The suspension turned brown within the first hour, indicating the formation of $HCoO_2$.

In the morning, the brown $HCoO_2$ product was isolated via centrifugation (15 min at 8200 g) and subjected to two cycles of [resuspension in ultrapure deionized water (40 mL) + centrifugation (15 min at 8200 g) + decantation]. The isolated materials were then resuspended in ultrapure deionized water (100 mL) and the resulting mixture was brought to reflux for two days to promote crystallization. After cooling to room temperature, the product was isolated from the suspension via centrifugation (15 min at 8200 g) and the wet pellet was freeze-dried on a lyophilizer to a constant weight. The resulting brown $HCoO_2$ powder was then annealed at 200 °C in a vacuum oven for one week, ensuring the temperature did not rise above 240 °C, where decomposition of the product to Co_3O_4 can occur.[39] (See SI for details regarding source and purity of materials.) Yield = 3.4 g.

Exfoliation and Dispersion of $[CoO_2]^-$ Nanosheets: The aforementioned annealed, crystalline $HCoO_2$ powder (50 mg) was added to a 100 mL round-bottom flask containing a concentrated aqueous TBA–OH solution (25 g of a 40 wt% mixture of TBAOH in water) and the whole mixture was shaken to suspend the powder. The resulting suspension was then sonicated with a solid tip VC 505 probe sonicator (500 W, Sonics & Materials, Inc., Newtown, CT) for 10 min (30% amplitude, 10 s pulses alternating with 10 s rest periods) to promote TBA intercalation into the lamellar $HCoO_2$ structure. The flask was then capped with a glass stopper and exfoliation was further promoted by vigorously stirring the sonicated mixture at 75 °C for four days. The exfoliated $[CoO_2]^-$ nanosheets were isolated from solution via ultracentrifugation (15 min at 15 000 g) and subjected to five cycles of [resuspension in ultrapure deionized water (20 mL) + centrifugation (15 min at 8200 g) + decantation] to remove residual TBA from solution. The isolated nanosheets were then redispersed in water (40 mL), where they were stable in solution to a moderate cycle centrifugation (15 min at 8200 g). Yield = 44 mg.

Fabrication of Thin-Film Cathodes: Self-supporting thin films of $[CoO_2]^-$ were prepared by VASA,[40] via filtration of the aforementioned aqueous $[CoO_2]^-$ nanosheet dispersion (≈1 mg mL^{-1}) through an Anodisc filter membrane (0.02 μm pore size). A Kontes Ultra-ware microfiltration apparatus with a fritted-glass support base was utilized for filtration. The fabricated films were washed by filtering through ultrapure deionized water (2×50 mL) then dried in air before removal from the filter membrane for characterization.

Ion Exchange: Exchange of protons for Li^+ was achieved following a modified literature procedure.[25] The VASA-fabricated thin film prepared in the previous experiment was submerged in an aqueous solution of $LiOH \cdot H_2O$ (20 mL, 0.25 or 2.5 M) at 160 °C under nitrogen pressure (900 psi) for five days in a 50 mL Parr reactor. ***Safety note***: The reactor was initially charged with nitrogen to 900 psi and then heated, which increases the pressure in the reactor. Thus, the reactor was gently, but quickly, vented every few minutes to bring the pressure back to 900 psi. When the reactor reached 160 °C and a final 900 psi pressure, it was left there for the remainder of the reaction.

Upon completion of the ion exchange, the reactor was cooled down and vented. The reaction mixture was then poured over a Büchner funnel lined with filter paper. Under vacuum, the collected thin film was then washed with ultrapure deionized water (5 × 50 mL) prior to further characterization.

Physical and Chemical Characterization: PXRD patterns were collected in the J. B. Cohen X-ray Diffraction Facility at Northwestern University (NU) with a Rigaku 2000 diffractometer (Rigaku Americas, The Woodlands, TX) using nickel filtered Cu Kα radiation (λ = 1.5406 Å). A cubic spline background was removed from all reported patterns.

HR-TEM images were collected in the NUANCE Facility at NU using a JEOL JEM-2100F FEG FasTEM (JEOL Ltd., Peabody, MA) at 200 kV. Samples were drop-cast onto a copper grid with a holey carbon support (Ted Pella, Inc., Redding, CA).

AFM images were also collected in the NUANCE facility using the tapping mode of a Nanoscope MultiMode Scanning Probe Microscope (Veeco Instruments, Inc., Plainview, NY) and a TESPA tip from Veeco corporation (Camarillo, CA). Samples were drop-cast onto a freshly cleaved mica substrate.

SEM images were gathered in the NEMS-MEMS Facility at NU using a field-emission gun Nova NanoSEM 600 microscope (FEI Co., Hillsboro, OR). Samples were coated with 6 nm of osmium using an OPC-60A osmium plasma coater (Structure Probe, Inc. Supplies, West Chester, PA) prior to analysis and affixed vertically to an aluminum stub with the fracture edge of the film toward the electron gun.

DLS measurements were collected using a Zetasizer Nano ZS (Malvern Instruments, Ltd., Worcestershire, UK) equipped with a He-Ne laser (633 nm). The noninvasive backscatter method (detection at 173° scattering angle) was used. The hydrodynamic diameters (D_H) of the nanosheets were calculated by the supplied instrument software (Zetasizer DTS) using the cumulant methods and the CONTIN algorithms. Molecular formulae for $Li_{1-x}H_xCoO_2$ were calculated from a combination of data from inductively coupled plasma-optical absorption spectroscopy and X-ray photoelectron spectroscopy (details in SI).

Electrochemical Characterization: Charge–discharge profiles and cycle performance data were collected at Argonne National Laboratory in a CR 2032-type coin-cell configuration using a Maccor battery cycler (Maccor, Inc., Tulsa, OK). Lithium metal foil served as the counter electrode and the electrolyte consisted of a mixture of ethylene carbonate and ethyl methyl carbonate (3:7 w/w) and lithium ions in the form of $LiPF_6$ (1.2 M in the carbonate mixture). All samples were heated at 75 °C for 3 h to remove residual moisture before being transferred to a He-filled glove box. Cells were charged and discharged at a current rate of 10 mA g^{-1}.

Supporting Information

Supporting Information is available from the Wiley Online Library or from the author.

Acknowledgements

This research was funded by the NSF (Award # DMR-0520513 through the Materials Research Science and Engineering Center at Northwestern University), US DOE (FreedomCAR and Vehicle Technologies Office), and ARO (Award # W991NF-09-1-0541). OCC is an NSF-ACC fellow (Award # CHE-0936924).

[1] J. M. Tarascon, M. Armand, *Nature* **2001**, *414*, 359–367.
[2] M. Endo, C. Kim, K. Nishimura, T. Fujino, K. Miyashita, *Carbon* **2000**, *38*, 183–197.
[3] M. Broussely, P. Biensan, B. Simon, *Electrochim. Acta* **1999**, *45*, 3–22.
[4] B. Scrosati, *Electrochim. Acta* **2000**, *45*, 2461–2466.
[5] K. Mizushima, P. C. Jones, P. J. Wiseman, J. B. Goodenough, *Mater. Res. Bull.* **1980**, *15*, 783–789.
[6] F. F. Lange, *J. Am. Ceram. Soc.* **1989**, *72*, 3–15.
[7] J. R. Dahn, E. W. Fuller, M. Obrovac, U. von Sacken, *Solid State Ionics* **1994**, *69*, 265–270.
[8] D. D. MacNeil, Z. Lu, Z. Chen, J. R. Dahn, *J. Power Sources* **2002**, *108*, 8–14.
[9] Y. Hernandez, V. Nicolosi, M. Lotya, F. M. Blighe, Z. Sun, S. De, I. T. McGovern, B. Holland, M. Byrne, Y. K. Gun'Ko, J. J. Boland, P. Niraj, G. Duesberg, S. Krishnamurthy, R. Goodhue, J. Hutchison, V. Scardaci, A. C. Ferrari, J. N. Coleman, *Nat. Nanotechnol.* **2008**, *3*, 563–568.
[10] A. Mourchid, A. Delville, J. Lambard, E. Lécolier, P. Levitz, *Langmuir* **1995**, *11*, 1942–1950.
[11] M. M. J. Treacy, S. B. Rice, A. J. Jacobson, J. T. Lewandowski, *Chem. Mater.* **1990**, *2*, 279–286.
[12] R. J. Smith, P. J. King, M. Lotya, C. Wirtz, U. Khan, S. De, A. O'Neill, G. S. Duesberg, J. C. Grunlan, G. Moriarty, J. Chen, J. Wang, A. I. Minett, V. Nicolosi, J. N. Coleman, *Adv. Mater.* **2011**, *23*, 3944–3948.
[13] Z. Tang, N. A. Kotov, S. Magonov, B. Ozturk, *Nat. Mater.* **2003**, *2*, 413–418.
[14] H. A. Becerril, J. Mao, Z. Liu, R. M. Stoltenberg, Z. Bao, Y. Chen, *ACS Nano* **2008**, *2*, 463–470.
[15] D. Li, M. B. Müller, S. Gilje, R. B. Kaner, G. G. Wallace, *Nat. Nanotechnol.* **2008**, *3*, 101–105.
[16] M. Yoshimura, *J. Mater. Res.* **1998**, *13*, 796–802.
[17] R. M. Fuoss, *Proc. Natl. Acad. Sci. USA* **1959**, *45*, 807–813.
[18] J. Akimoto, Y. Gotoh, Y. Oosawa, *J. Solid State Chem.* **1998**, *141*, 298–302.
[19] O. C. Compton, E. C. Carroll, J. Y. Kim, D. S. Larsen, F. E. Osterloh, *J. Phys. Chem. C* **2007**, *111*, 14589–14592.
[20] Upon prolonged standing, a small amount of larger particles can sometimes settle out of solution but can be readily redispersed by gentle shaking.
[21] P. Nemes-Incze, Z. Osváth, K. Kamarás, L. P. Biró, *Carbon* **2008**, *46*, 1435–1442.
[22] S. H. Choi, J. Kim, Y. S. Yoon, *J. Power Sources* **2004**, *135*, 286–290.
[23] J. M. Serratosa, W. D. Johns, A. Shimoyama, *Clays Clay Min.* **1970**, *18*, 107–113.
[24] Y. D. Kondrashev, N. N. Fedorova, *Dokl. Akad. Nauk* **1954**, *94*, 229–231.
[25] D. Larcher, M. R. Palacín, G. G. Amatucci, J. M. Tarascon, *J. Electrochem. Soc.* **1997**, *144*, 408–417.
[26] S. P. Sheu, C. Y. Yao, J. M. Chen, Y. C. Chiou, *J. Power Sources* **1997**, *68*, 533–535.
[27] S. Choi, A. Manthiram, *J. Electrochem. Soc.* **2002**, *149*, A162–A166.
[28] J. Li, E. Murphy, J. Winnick, P. A. Kohl, *J. Power Sources* **2001**, *102*, 294–301.
[29] J. Xie, N. Imanishi, T. Matsumura, A. Hirano, Y. Takeda, O. Yamamoto, *Solid State Ionics* **2008**, *179*, 362–370.
[30] C. G. Wu, D. C. DeGroot, H. O. Marcy, J. L. Schindler, C. R. Kannewurf, Y. J. Liu, W. Hirpo, M. G. Kanatzidis, *Chem. Mater.* **1996**, *8*, 1992–2004.
[31] J. N. Reimers, J. R. Dahn, *J. Electrochem. Soc.* **1992**, *139*, 2091–2097.
[32] M. Itagaki, N. Kobari, S. Yotsuda, K. Watanabe, S. Kinoshita, M. Ue, *J. Power Sources* **2005**, *148*, 78–84.
[33] Y.-I. Jang, B. Huang, H. Wang, D. R. Sadoway, Y.-M. Chiang, *J. Electrochem. Soc.* **1999**, *146*, 3217–3223.
[34] W. Li, J. N. Reimers, J. R. Dahn, *Solid State Ionics* **1993**, *67*, 123–130.
[35] J. Cho, Y. J. Kim, B. Park, *Chem. Mater.* **2000**, *12*, 3788–3791.
[36] H. Zhao, L. Gao, W. Qiu, X. Zhang, *J. Power Sources* **2004**, *132*, 195–200.
[37] A. Mauger, X. Zhang, H. Groult, C. M. Julien, *ECS Meeting Abstracts* **2011**, *1101*, 583.
[38] M. Figlarz, J. Guenot, J. N. Tournemolle, *J. Mater. Sci.* **1974**, *9*, 772–776.
[39] S. Kittaka, N. Uchida, I. Miyashita, T. Wakayama, *Colloids Surf.* **1989**, *37*, 39–54.
[40] K. W. Putz, O. C. Compton, M. J. Palmeri, S. T. Nguyen, L. C. Brinson, *Adv. Funct. Mater.* **2010**, *20*, 3322–3329.

Received: June 8, 2011
Published online: February 8, 2012